Journal of Nuclear Medicine, published on August 25, 2022 as doi:10.2967/jnumed.122.264213

Differential effects of tau stage, Lewy body pathology, and substantia nigra degeneration on FDG-PET patterns in clinical AD

Jesús Silva-Rodríguez[1], Miguel A. Labrador-Espinosa[1,2,3], Alexis Moscoso[4], Michael Schöll[4], Pablo Mir[1,2,3,*] and Michel J. Grothe[1,2,4,*] for the Alzheimer's Disease Neuroimaging Initiative[+]

Affiliations:

[1] Unidad de Trastornos del Movimiento, Servicio de Neurología y Neurofisiología Clínica, Instituto de Biomedicina de Sevilla, Hospital Universitario Virgen del Rocío/CSIC/Universidad de Sevilla, Seville, Spain.

[2] Centro de Investigación Biomédica en Red sobre Enfermedades Neurodegenerativas (CIBERNED), Madrid, Spain.

[3] Departamento de Medicina, Facultad de Medicina, Universidad de Sevilla, Seville, Spain.

[4] Wallenberg Center for Molecular and Translational Medicine and Department of Psychiatry and Neurochemistry, University of Gothenburg, Gothenburg, Sweden.

[+] Data used in preparation of this article were obtained from the Alzheimer's Disease Neuroimaging Initiative (ADNI) database. A complete listing of ADNI investigators can be found at: http://adni.loni.usc.edu/wp-content/uploads/how_to_apply/ADNI_Acknowledgement_List.pdf

[*] **Corresponding authors:**

Pablo Mir, MD, PhD. E-mail: pmir@us.es

Michel Grothe, PhD. Email: mgrothe@us.es

Unidad de Trastornos del Movimiento, Instituto de Biomedicina de Sevilla, Hospital Universitario Virgen del Rocío, Avda. Manuel Siurot s/n, 41013, Seville, Spain;

***Keywords*:** FDG, LBD, AD, autopsy

ABSTRACT:

Purpose: Comorbid Lewy body (LB) pathology is common in AD. The effect of LB co-pathology on FDG-PET patterns in AD is yet to be studied. We analysed associations of neuropathologically-assessed tau pathology, LB pathology, and substantia nigra neuron loss (SNnl) with ante-mortem FDG-PET hypometabolism in patients with a clinical AD presentation.

Methods: Twenty-one patients with autopsy-confirmed AD ('pure-AD'), 24 with AD and LB co-pathology ('AD-LB'), and 7 with LB but no or low evidence of AD pathology ('pure-LB') were studied. Pathologic groups were compared on regional and voxel-wise FDG-PET patterns, the cingulate island sign ratio (CISr), and neuropathological ratings of SNnl. Additional analyses assessed continuous associations of Braak tangle stage and SNnl with FDG-PET patterns.

Results: Pure-AD and AD-LB showed highly similar patterns of AD-typical temporo-parietal hypometabolism and did not differ in CISr, regional FDG SUVR, or SNnl. By contrast, pure-LB showed the expected DLB-like pattern, accompanied by pronounced occipital hypometabolism and elevated CISr and SNnl compared to the AD groups. In continuous analyses, Braak tangle stage was significantly correlated with more AD-like, and SNnl with more DLB-like, FDG-PET patterns.

Conclusions: In autopsy-confirmed AD dementia patients, comorbid LB pathology did not have a notable effect on the regional FDG-PET pattern. A more DLB-like FDG-PET pattern was observed in relation to SNnl, but advanced SNnl was mostly limited to relatively pure LB cases. AD pathology may have a dominant effect over LB pathology in determining the regional neurodegeneration phenotype.

Introduction

Alzheimer's disease (AD) and dementia with Lewy bodies (DLB) are two distinct neurodegenerative conditions defined by the cerebral accumulation of amyloid-β plaques and tau neurofibrillary tangles (NFT), and alpha-synuclein containing Lewy bodies (LB), respectively (*1*,*2*). In contrast to AD, DLB typically presents with denervation of the nigrostriatal dopaminergic pathway caused by degeneration of dopaminergic substantia nigra neurons (*3*), as well as more predominant executive and visuospatial deficits accompanied by visual hallucinations, cognitive fluctuations, parkinsonism, and REM sleep behavioural disorder (*4*). Although AD and DLB have unique neuropathological profiles, up to 60% of clinical AD and DLB patients present with neuropathological findings of both diseases (*5*,*6*). Concomitant LB pathology in clinical AD has been associated with faster cognitive decline (*7*–*9*), younger age at death (*8*), and more DLB-like clinical features (*9*–*12*), although this could not be confirmed by others (*7*,*13*,*14*). In the era of disease-modifying therapies, these patients may benefit less from amyloid-lowering therapies (*15*), whereas they may potentially show a better response to cholinesterase inhibitors (*16*). Biomarkers identifying these patients may thus allow for a more targeted treatment of AD (*11*,*17*).

Positron Emission Tomography (PET) with glucose analogue [18F]fluorodeoxyglucose (FDG) is a well-established modality for imaging neurodegeneration, and differentiated hypometabolism patterns have been established for different conditions (*18*). Particularly, in contrast to the characteristic temporo-parietal pattern of hypometabolism in AD, patients with DLB are characterized by a more pronounced posterior-occipital pattern of hypometabolism with relatively preserved metabolism in the medial temporal lobe (MLT) and also in the posterior cingulate, the latter known as the cingulate island sign (CIS) (*19*,*20*). The CIS is a well-established biomarker for distinguishing patients with DLB and AD (*19*,*21*), even at prodromal stages (*22*).

Previous imaging-pathologic association studies have demonstrated that AD co-pathology in DLB associates with a less DLB-typical hypometabolic pattern (*20*,*23*), but the potential contributions of FDG-PET to the identification of mixed pathology in AD-like presentations are yet to be explored. Here, we assessed ante-mortem FDG-PET patterns of clinically diagnosed AD patients in relation to AD and LB neuropathology at autopsy.

Methods

Study participants

Our cohort included 59 participants enrolled in the Alzheimer's Disease Neuroimaging Initiative (ADNI, adni.loni.usc.edu) who had neuropathological examinations at autopsy, a clinical diagnosis of AD dementia or amnestic mild cognitive impairment (aMCI) at last clinical evaluation, and available ante-mortem FDG-PET scans. The average interval between the last available FDG-PET acquisition and death was 3.0 ± 2.6 years.

Neuropathological assessments

Neuropathological assessments were performed by the ADNI Neuropathology Core following the NIA-AA guidelines (*24–26*). Standard rating scales for AD pathology (amyloid, tau, neuritic plaques) were further merged into the AD neuropathologic change (ADNC) composite, while LB pathology assessment followed the McKeith criteria (*4*). Patients were considered to have autopsy-confirmed AD when presenting intermediate or high ADNC (*24*), and presence of LB neuropathological changes (LBNC) was denoted when LBs were present in limbic or neocortical regions or the amygdala (*4*). Amygdala-predominant LBs, which have been suggested to be characteristic of advanced AD and less likely related to DLB (*27*), were considered as positive LBNC. Patients with LBNC restricted to the brainstem were excluded. Patients were stratified as autopsy-confirmed AD without LBNC (pure-AD), autopsy-confirmed AD with comorbid LBNC (AD-LB), LBNC without fulfilling neuropathologic criteria for AD (pure-LB), or none (Negative). We also studied semi-quantitative ratings (assessed on a scale from 0 to 3) of substantia nigra neuronal loss (SNnl) as a marker of DLB-specific neurodegeneration (*4*,*28*). For a subset of patients (n=45/59), semiquantitative ratings of the regional loads of tau NFTs and LBs were available (See Supplementary Table S1).

Genetics

APOE genotype was determined by Cogenics using standard methods to genotype the two APOE-ε4-defining SNPs (rs429358, rs7412). Patients were labelled as having zero, one or two ε4 copies.

Neuropsychological evaluation

The Mini-Mental State Evaluation (MMSE) was used for characterizing global cognitive performance (*29*). Domain-specific composite scores were used for assessing memory (ADNI-MEM) (*30*) and executive function (ADNI-EF) (*31*). In addition, we calculated a "cognitive profile" variable Δ(MEM-EXEC) to characterize relative impairments between these two domains (*32*). The average interval between neuropsychological evaluation and death was 1.9 ± 2.0 years.

FDG-PET acquisition and processing

For this work, we used FDG-PET images in fully pre-processed format (level four) as provided by ADNI. Details of acquisition and pre-processing are detailed elsewhere (http://adni.loni.usc.edu/methods/pet-analysis-method/pet-analysis/). Blood glucose levels (BGL), previously associated with changes in posterior-occipital hypometabolism (*33*), are reported. FDG-PET images were spatially normalized using SPM12 (fil.ion.ucl.ac.uk/spm/software/spm12) and scaled using a previously validated data-driven method (*34*) to FDG-PET data from 179 cognitively normal ADNI subjects (henceforth, the "control group"). Region-of-interest (ROI) analysis was performed to calculate the average FDG uptake in the occipital cortex and the MTL (*21*), and also the CIS ratio (CISr) (*20*,*22*) between the posterior cingulate cortex and the precuneus and cuneus uptake. To this end, we used the corresponding ROIs from the Harvard-Oxford neuroanatomical atlas.

Statistical analysis

Two-sample t-tests and Mann-Whitney U tests were used for comparing normally distributed continuous variables and non-normally distributed and ordinal variables, respectively. Effect sizes were reported as Cohen's d.

Hypometabolism patterns were determined by voxel-wise two-sample t-tests between each pathologic group and the control group using SPM. Age, sex, and blood glucose levels (BGL) were used as confounding nuisance covariates (*33*,*35*). T-score maps were transformed to Cohen's d-maps and thresholded by $p<0.05$ (FDR), $k>250$ voxels. For secondary analysis, the AD-LB group was separated into AD with amygdala-

predominant LBs and AD with limbic or neocortical LBs. Direct comparisons between the different pathological groups were also performed. Spatial similarities between hypometabolism patterns were assessed using spatial Spearman's correlation analysis across the 52 ROIs defined in the Harvard-Oxford atlas (*36*).

In addition, we performed regional and voxel-wise Spearman correlation analyses of the association between AD- (Braak tau stage) and DLB-specific (SNnl) neuropathologic markers and FDG-PET patterns. In complementary analyses, we also assessed associations between FDG-PET and semi-quantitative ratings of regional LB and NFT load (See Supplementary Material).

Results

Demographics and neuropathology

Seven subjects (11.9%) did not fulfil the criteria for either ADNC or LBNC, including two cases that had LBs restricted to the brainstem (and ADNC≤1). Of the remaining 52 subjects, twenty-one (35.6%) had autopsy-confirmed AD without LBNC (pure-AD), twenty-four (40.7%) had autopsy-confirmed AD with LBNC co-pathology (AD-LB), and seven (11.9%) had LBNC without fulfilling pathologic criteria for AD (ADNC≤1) (pure-LB). Among AD-LB, sixteen patients presented limbic/transitional or neocortical LBNC (67%), while eight patients presented amygdala-predominant LBNC (33%).

Patients in the pure-AD and AD-LB groups did not differ with respect to age, sex, *APOE* ε4 positivity, or BGL, but pure LB patients were significantly older (p=0.039) and less often carriers of the *APOE* ε4 allele (p=0.018) compared to the other groups (Table 1). Regarding neuropathology, the pure-AD and the AD-LB groups did not differ in severity of Braak stages (p=0.695) or regional NFT burden (Suppl. Fig. S1). Amygdala-predominant LBs were significantly more frequent in the AD-LB than in the pure-LB group (p=0.047), but semiquantitative ratings of regional LB burden did not differ between these groups (Suppl. Fig. S1). Finally, SNnl was significantly higher for pure-LB than for pure-AD (p=0.005) and AD-LB (p=0.020) but similar between AD and AD-LB (p=0.210).

In terms of cognition, there were no significant differences in MMSE between groups, but patients in the AD-LB group showed significantly worse memory performance than pure-AD (p=0.012) and pure-LB (p=0.004), while executive function was similar between groups. Accordingly, AD-LB subjects showed a memory-predominant cognitive profile in Δ(MEM-EXEC) (1-sample t-test, p=0.045), whereas pure-LB subjects showed a disproportionate executive impairment (p=0.057), and pure-AD cases showed balanced deficits in both domains (p=0.161). Limbic LB load was negatively correlated with ADNI_MEM (after correcting for the effect of tau NFT burden) across the whole cohort, but not in the AD-LB group alone (Supplementary Table S2).

	Pure-AD (n=21)	**AD-LB (n=24)**	**Pure-LB (n = 7)**
Age at death, y	81.8±7.7	81.0±8.4	88.6±4.9
Imaging to death, y	2.3±3.5	3.3±3.0	3.1±2.7
MCI/Dementia (at death)	3/18	1/23	2/5
Male/Female	12/8	19/5	6/1
APOE ε4 --/+-/++	9/11/1	7/11/6	6/0/0
Braak stage (I-IV/V/VI)	3/14/5	1/18/5	7/0/0
Lewy bodies (limbic/neocortical/amygdala)	0/0/0	2/14/8	1/6/0
SNnl	0.86±0.47	1.04±0.46	1.57±0.49
FDG-PET BGL (mg/dl)	101.7±11.7	97.8±19.9	94.4±8.2
MMSE score	22.4±6.6	21.5±5.7	24.7±3.9
ADNI_MEM	-1.06±0.94	-1.61±0.66	-0.69±0.67
ADNI_EXEC	-1.36±1.21	-1.48±0.95	-1.50±0.95
Δ (MEM - EXEC)	0.16±0.50	-0.33±0.71	0.53±0.55

Table 1: Demographic characteristics of the different pathologic subgroups.

FDG patterns of pathologically defined groups

Compared to healthy controls, the pure-AD group showed the classical AD hypometabolism pattern, with pronounced medial and lateral temporal effects extending to the lateral parietal cortex, posterior cingulate and precuneus, mild frontal hypometabolism and well-preserved occipital metabolism (Fig. 1a). The mixed pathology AD-LB group was characterized by a spatial pattern remarkably similar to the pure-AD group (spatial correlation: ρ=0.82). Interestingly, the same pattern was also observed when analyzing AD-LB cases with limbic/neocortical or amygdala-predominant LB separately (Fig. 1b). By contrast, the pure-LB group showed the typical DLB pattern of pronounced posterior-occipital hypometabolism with relative sparing of the MTL and the posterior cingulate, which as expected was not spatially correlated with the pure-AD pattern (ρ=0.09). In direct comparisons, only non-significant differences were observed between the pure-AD and AD-LB groups, while the pure-LB group showed significant posterior-occipital hypometabolism and a relative sparing of frontal and temporal regions in comparison to both pure-AD and AD-LB (Fig. 1c).

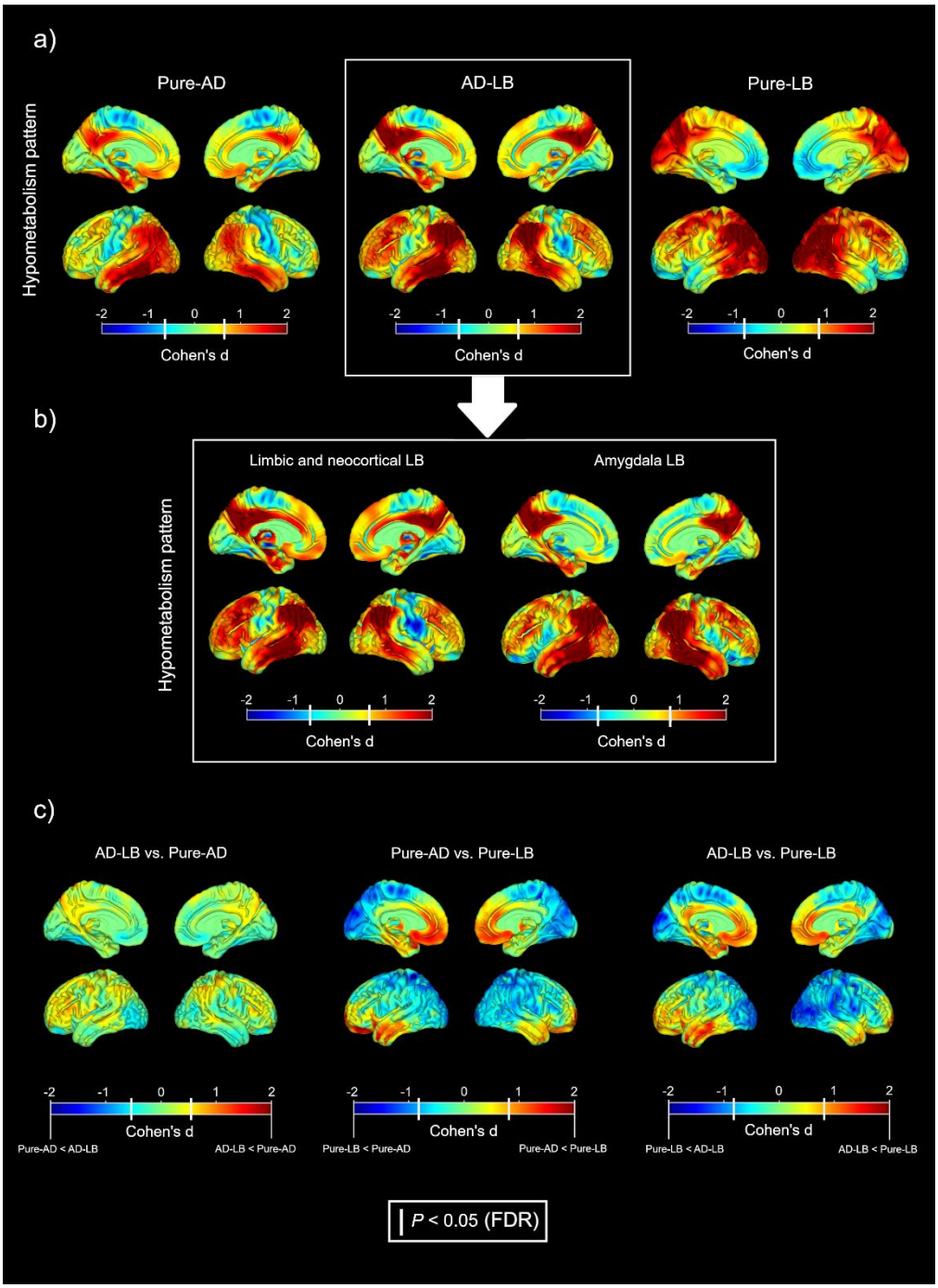

Fig. 1: *a)* Hypometabolism patterns of the pathologic groups compared to controls. *b)* Patterns of the limbic/neocortical and amygdala-predominant Lewy body subgroups in AD-LB. c) Direct comparisons between the pathologic groups. Color represents effect size. White bars in color bars: p<0.05 (FDR).

ROI-based analyses fully reproduced and quantified the voxel-wise observations, revealing significant MTL hypometabolism in the pure-AD and AD-LB groups, and occipital hypometabolism in the pure-LB group (Fig. 2).

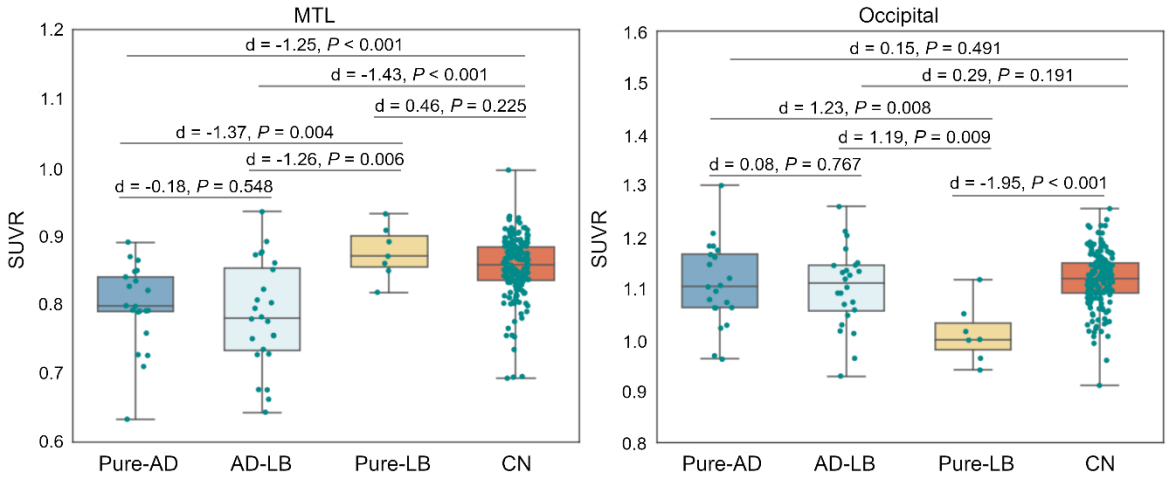

Fig. 2: Comparison of medial temporal lobe (MTL) and occipital cortex FDG standard uptake value ratios (SUVR) between the different neuropathological groups and the control group.

Additionally, patients in the pure-LB group exhibited significantly higher CISr than those in the pure-AD (d=0.78, p=0.010) and the AD-LB (d=0.95, p=0.002) groups (pure-AD vs. AD-LB: d=0.15, p=0.375) (Fig. 3a). CISr was also similar for limbic/neocortical and amygdala-predominant LBs (d=0.18, p=0.516). By contrast, patients with an elevated SNnl (≥2) showed a significantly higher CISr (d=1.49, p<0.001), even when considering only the pure-AD and AD-LB groups (d=1.31, p=0.016). Moreover, individual z-score maps of the three AD-LB patients with elevated SNnl revealed a more prominent DLB-like or mixed hypometabolism pattern (Fig. 3b; spatial correlations: case #1: ρ=0.82 and ρ=0.26; case #2: ρ=0.57 and ρ=0.17; case #3: ρ=0.57 and ρ=0.41, for the pure-LB and pure-AD patterns, respectively).

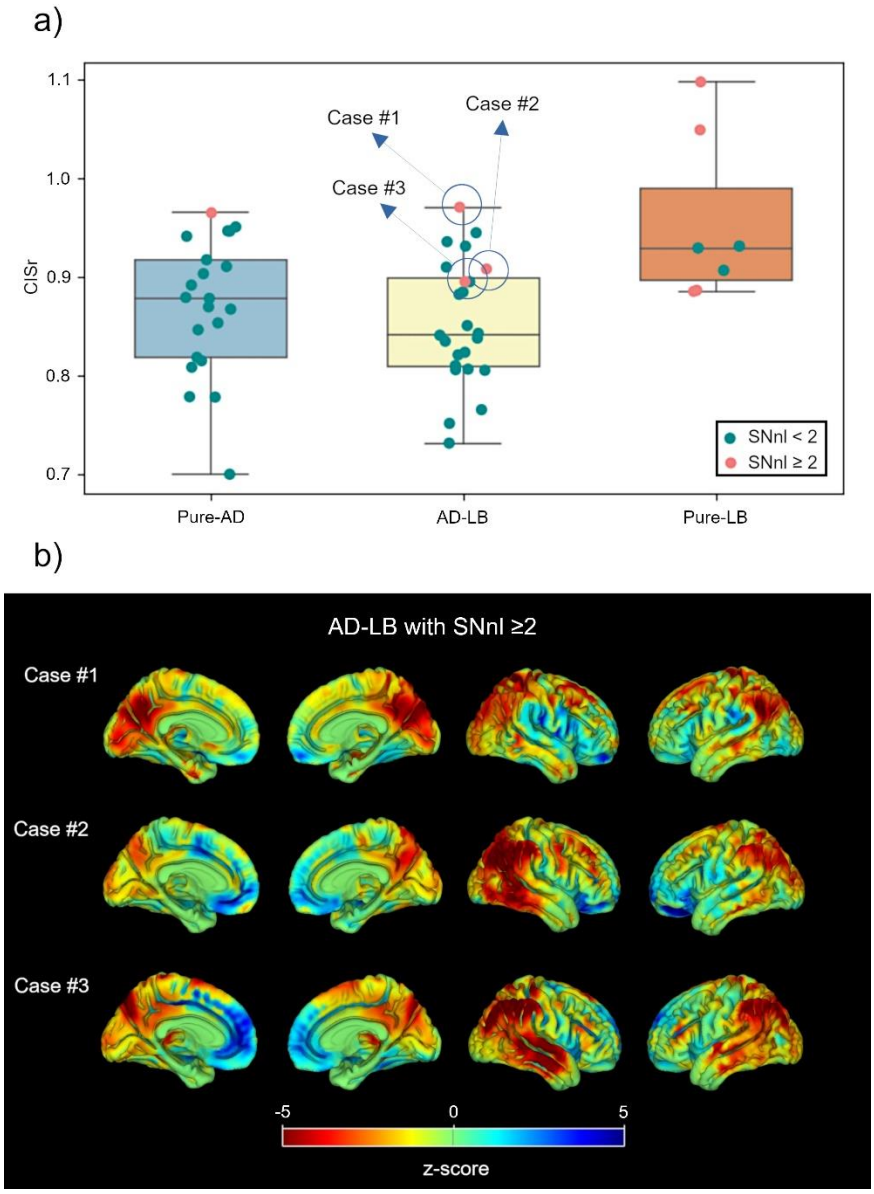

Fig. 3: (a) CISr comparisons between the pathologic groups. Cases with high SNnl ≥2 are highlighted in orange. (b) Individual z-score maps of the three AD-LB cases with high SNnl.

Continuous associations of Braak tau stage and SNnl with FDG-PET patterns

To better understand the role of AD- and DLB-specific neuropathologic markers in shaping the observed FDG-PET patterns, we studied the continuous associations between Braak tau stage and SNnl and FDG-PET ROI values across the full sample (Fig. 4). Braak stage was negatively correlated with the CISr and MTL

metabolism, whereas SNnl was positively correlated with the CISr but negatively correlated with occipital metabolism. In complementary analysis, similar associations with regional FDG-PET markers were observed when using regional tau NFT loads instead of Braak stage (Suppl. Fig. S2), but regional LB burden was not significantly correlated with FDG-PET features (Suppl. Fig. S3).

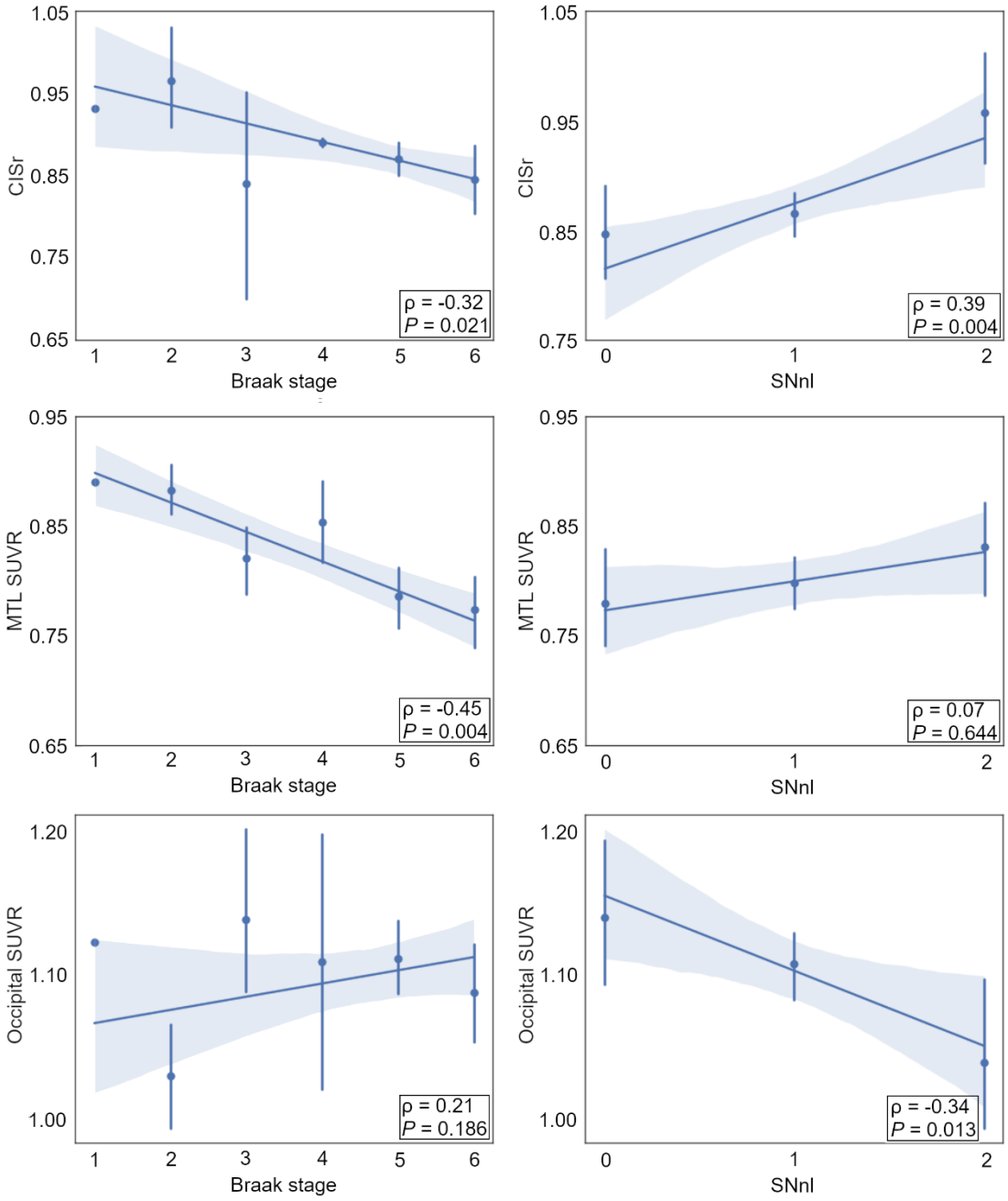

Fig. 4: Correlations of Braak tau stage and SNnl with regional FDG-PET markers. *Left*: Braak tau stage. *Right*: SNnl. *Top:* CISr. *Middle:* MTL SUVR. *Bottom:* Occipital SUVR.

In additional voxel-wise analyses, higher Braak stages were correlated with more hypometabolism in the posterior cingulate, MTL, and temporo-parietal cortex, as well as with less hypometabolism in the occipital and the paracentral cortex (Fig. 5, top). SNnl was correlated with more hypometabolism in occipital and parieto-temporal regions, and less hypometabolism in the orbitofrontal cortex and the posterior cingulate (Fig. 5, bottom).

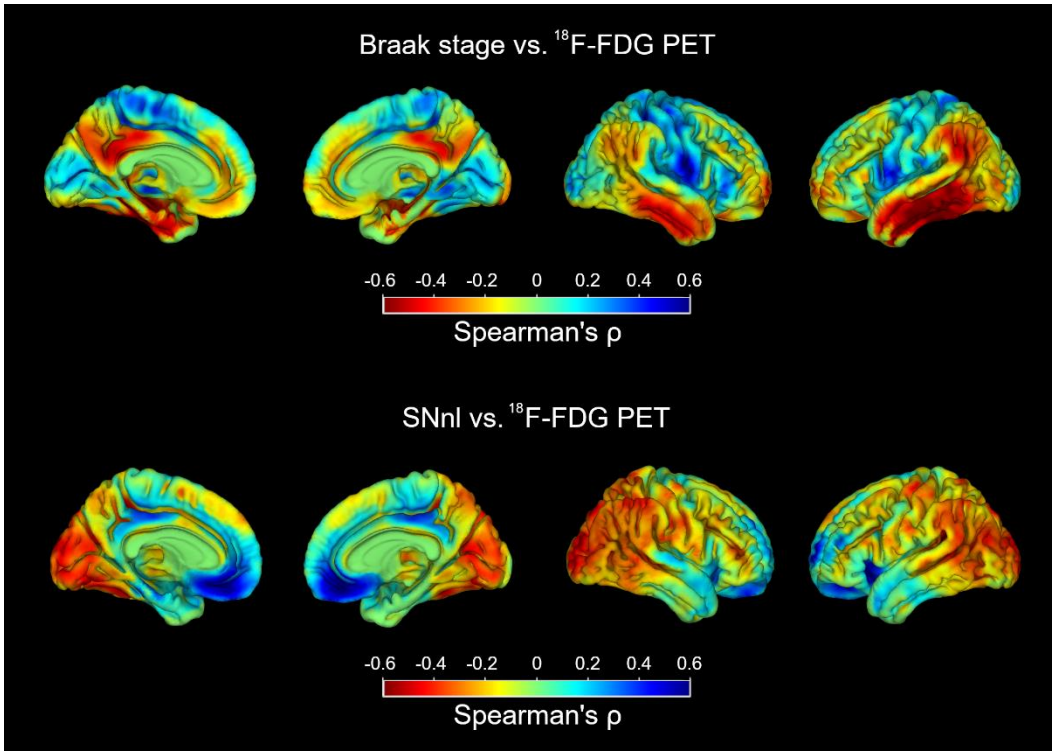

Fig. 5: Voxel-wise correlations of Braak tau stage (top) and SNnl (bottom) with FDG uptake.

Discussion

In the present work we analyzed ante-mortem FDG-PET patterns in relation to AD and LB pathology in a cohort of clinical AD patients. In our study, concomitant AD-LB patients did not show more DLB-like FDG-PET features, but rather a pattern regionally very similar to the pure-AD pattern (Fig. 1, Fig. 2). Accordingly,

the CISr (*20–22*) did not differ between pure-AD and AD-LB (Fig. 3). In contrast to our results, in a previous work comparing pathologically verified DLB (n=3) and AD-LB (n=3) patients (*37*), the authors reported similar occipital hypometabolism in both groups. These differences may be explained by different definitions of the AD-LB group, since AD-LB patients in this previous work presented with DLB symptomatology compared to the relatively pure AD phenotype in our study. Interestingly, the amygdala-predominant LB type, which has been previously linked to AD (*27*) was indeed higher in the AD-LB group compared to the pure-LB group (where it was completely absent), but this did not seem to affect the neurodegeneration phenotype (Fig. 1b). While the little effect of comorbid LB pathology on the regional FDG-PET pattern may come as a surprise, it is also in line with the lack of elevated SNnl, a pathologic hallmark of LB-typical neurodegeneration, in these comorbid AD-LB cases (*28*,*38*).

While AD-LB patients showed an even more amnestic-predominant cognitive profile compared to pure AD, rather than a more dysexecutive phenotype typical for DLB (*4*), this difference is unlikely to result from a more advanced AD pathology in the AD-LB group, as severity of both Braak stage (Table 1) and regional NFT burden (Suppl. Fig. S1) were comparable between pure-AD and AD-LB. Previous studies have similarly suggested that co-morbid LB pathology exacerbates AD-typical cognitive deficits but does not necessarily produce a mixed clinical phenotype (*7*,*13*,*14*), while others did observe more DLB symptomatology in AD-LB cases (*8–12*,*39*). These differences may be explained by different clinico-pathologic definitions of the AD-LB groups, as some autopsy studies define the different pathology groups based solely on neuropathologic criteria (*8*,*39*), while others also restrict their samples to a particular clinical phenotype as in our study (*6*,*13*,*20*,*23*).

Interestingly, a smaller group of patients (12%) who had relatively pure LBNC with no or low ADNC did indeed show the expected DLB-like posterior-occipital hypometabolism pattern (*20*), which was accompanied by significantly elevated SNnl. Moreover, quantitative neuropsychological analysis these patients had a more dysexecutive rather than amnestic-predominant profile. Thus, it is likely that these cases may reflect misdiagnosed DLB patients with no DLB-specific symptomatology and a clinical profile more similar to AD (*4*,*40*). Our findings indicate that FDG-PET may serve as a very useful imaging marker to identify this non-negligible and clinically highly relevant portion of misdiagnosed AD patients in-vivo. Interestingly, despite

having similar regional loads of LB pathology (Suppl. Fig. S1), the co-morbid AD-LB group did not exhibit a DLB-like FDG-PET pattern or elevated SNnl, suggesting that AD pathology may have a dominant effect over LB pathology in determining the regional neurodegeneration phenotype in these patients. Altogether, these results suggest that LBs may play a different role in AD-LB compared to pure-LB. While recent studies have provided evidence of in-vivo interactions between tau and alpha-synuclein (*41*), more work needs to be done to better understand how these interactions may modify the effect of LB pathology on the neurodegeneration phenotype in AD-LB.

In continuous association analyses we observed that Braak stage (Fig. 4, Fig.5) and tau NFT load (Suppl. Fig. S2) were significantly correlated with more AD-like FDG-PET features, confirming and expanding recent findings obtained in a smaller subsample of the ADNI autopsy cohort (*42*) and also similar observations previously reported in clinical DLB (*20*,*23*). Interestingly, SNnl showed the opposite pattern of associations, being associated with a higher CISr, lower occipital SUVR, as well as with a more DLB-like hypometabolism pattern in voxel-wise analysis (Fig. 4, Fig. 5). Most interestingly, this association was even observed on an individual basis in a small subset of AD-LB patients that did have advanced SNnl (Fig. 3b). Nevertheless, this applied only to three AD-LB cases (12.5%), suggesting that comorbid LB rarely affects the neurodegeneration phenotype in cases with fully developed AD pathology. More research is necessary to better understand the neurobiological factors that determine why comorbid LB pathology leads to SNnl and a DLB-typical neurodegeneration pattern in some patients but not in others (*43*).

Altogether, our results suggest that it may not be the presence of LB pathology by itself, but rather the associated SNnl that links with a more DLB-like hypometabolic pattern in these clinical AD patients. This notion was further corroborated by the fact that semi-quantitative ratings of regional LB burden were not significantly associated with FDG-PET markers (Supp. Fig. S3). To the best of our knowledge, our study is the first report demonstrating these associations. A very recent multimodal neuroimaging study (n=55) has pointed to an association between nigrostriatal degeneration (as assessed by dopamine transporter SPECT) and cortical hypometabolism in clinical DLB (*44*). However, such associations had neither been assessed using neuropathologic evaluations nor in the context of clinical AD. Additional studies combining FDG-PET

with imaging modalities aimed to evaluate SN degeneration in-vivo (*44–47*) would be of great interest for replicating and studying these associations in larger observational cohorts.

Regarding the clinical implications of our work, our novel finding of comparable FDG-PET patterns in AD-LB and pure AD suggests that FDG-PET may not be able to readily detect comorbid LB pathology in AD patients, which may be a disappointing finding that is nevertheless of utmost clinical relevance. While larger studies might be useful to corroborate these findings, the comparably large sample used here (n=21 pure AD vs n=23 AD-LB) and the low effect size estimates indicate that this finding would be unlikely to change with higher sample sizes. However, according to our findings FDG-PET may be very useful for identifying a subset of clinically diagnosed AD patients who have relatively pure LB pathology, as well as those pathologic AD patients where the comorbid LB pathology is accompanied by SN neurodegeneration. Identifying these patients has important clinical implications as these will most likely also show different clinical trajectories (*7*), including development of more DLB-typical symptomatology (*9*) and possibly also the typical susceptibility to antagonistic dopaminergic neuroleptics known for DLB patients (*48*).

Our work also presents a series of limitations. First, the restriction on patients with typical AD-like clinical presentations limits the reach of our conclusions to this particular clinical setting, and different effects of comorbid AD-LB pathology may be observed in clinically more diverse dementia cohorts (*8*). Nevertheless, identifying (co-morbid) LB pathology in clinical AD patients poses a distinct diagnostic challenge that has a potentially high relevance for individual patient management and recruitment into AD clinical trials (*6*) that had not been addressed so far using FDG-PET. In close relation, neuropsychological data collected within the ADNI study allows for the assessment of a specific dysexecutive or amnestic-predominant neuropsychological profile, but DLB core features are not assessed in enough detail (or not assessed at all). Finally, quantitative assessments of regional pathologic load may represent a closer pathologic correlate of phenotypic differences than the standardized semi-quantitative rating scales employed here (*43*).

Conclusions

FDG-PET may not be able to readily detect comorbid LB pathology in clinical AD, but it may be very useful for identifying a subset of patients with prominent LB-related neurodegeneration, which may have important implications for patient management, individualized disease prognosis, and selection for treatment trials.

Disclosure

This work was supported by the Instituto de Salud Carlos III (ISCIII-FEDER, PI19/01576, PI20/00613) and the Junta de Andalucía (CVI-02526, CTS-7685, PE-0186-2019, PI-0046-2021). JSR is a “Sara Borrell” fellow (CD21/00067) and MJG is a “Miguel Servet” fellow (CP19/00031). MALE is supported by VI-PPIT-US (University of Seville, USE-19094-G). AM is supported by Gamla Tjänarinnor. MS is supported by the Knut and Alice Wallenberg Foundation (KAW 2014.0363), the Swedish Research Council (#2017-02869), the Swedish state under the ALF-agreement (#ALFGBG-813971) and the Swedish Alzheimer Foundation (#AF-740191). Data collection and sharing for this project was funded by the ADNI, a public-private partnership program supported by national as well as contributions from several companies (https://adni-dup.loni.usc.edu/about/funding/)

KEY POINTS:

QUESTION: Is the presence of Lewy body pathology, or related substantia nigra neurodegeneration, associated with a differential FDG-PET pattern in clinical AD?

PERTINENT FINDINGS: LB co-pathology did not affect the FDG-PET pattern in autopsy-confirmed AD, but a distinct posterior-occipital FDG-PET pattern was observed in relation to substantia nigra degeneration, which was mostly observed in clinical AD cases with relatively pure LB pathology at autopsy.

IMPLICATIONS FOR PATIENT CARE: FDG-PET can identify clinically diagnosed AD patients that have relatively pure LB pathology and substantia nigra neurodegeneration at autopsy. In-vivo identification of these patients has important implications for clinical patient management, individualized disease prognosis, and selection for treatment trials.

REFERENCES

1. Kövari E, Horvath J, Bouras C. Neuropathology of Lewy body disorders. *Brain Res Bull*. 2009;80:203-210.

2. Perl DP. Neuropathology of Alzheimer's disease. *Mt Sinai J Med N Y*. 2010;77:32-42.

3. Seidel K, Mahlke J, Siswanto S, et al. The brainstem pathologies of Parkinson's disease and dementia with Lewy bodies. *Brain Pathol Zurich Switz*. 2015;25:121-135.

4. McKeith IG, Boeve BF, Dickson DW, et al. Diagnosis and management of dementia with Lewy bodies: Fourth consensus report of the DLB Consortium. *Neurology*. 2017;89:88-100.

5. J. Irwin D, I. Hurtig H. The Contribution of Tau, Amyloid-Beta and Alpha-Synuclein Pathology to Dementia in Lewy Body Disorders. *J Alzheimer's Dis Park*. 2018;08.

6. Robinson JL, Richardson H, Xie SX, et al. The development and convergence of co-pathologies in Alzheimer's disease. *Brain J Neurol*. 2021;144:953-962.

7. Malek-Ahmadi M, Beach TG, Zamrini E, et al. Faster cognitive decline in dementia due to Alzheimer disease with clinically undiagnosed Lewy body disease. Ginsberg SD, ed. *PLOS ONE*. 2019;14:e0217566.

8. Chung EJ, Babulal GM, Monsell SE, Cairns NJ, Roe CM, Morris JC. Clinical Features of Alzheimer Disease With and Without Lewy Bodies. *JAMA Neurol*. 2015;72:789.

9. Chatterjee A, Hirsch-Reinshagen V, Moussavi SA, Ducharme B, Mackenzie IR, Hsiung GR. Clinico-pathological comparison of patients with autopsy-confirmed Alzheimer's disease, dementia with Lewy bodies, and mixed pathology. *Alzheimers Dement Diagn Assess Dis Monit*. 2021;13.

10. Savica R, Beach TG, Hentz JG, et al. Lewy body pathology in Alzheimer's disease: A clinicopathological prospective study. *Acta Neurol Scand*. 2019;139:76-81.

11. Thomas AJ, Mahin-Babaei F, Saidi M, et al. Improving the identification of dementia with Lewy bodies in the context of an Alzheimer's-type dementia. *Alzheimers Res Ther*. 2018;10:27.

12. Azar M, Chapman S, Gu Y, Leverenz JB, Stern Y, Cosentino S. Cognitive tests aid in clinical differentiation of Alzheimer's disease versus Alzheimer's disease with Lewy body disease: Evidence from a pathological study. *Alzheimers Dement J Alzheimers Assoc*. 2020;16:1173-1181.

13. Roudil J, Deramecourt V, Dufournet B, et al. Influence of Lewy Pathology on Alzheimer's Disease Phenotype: A Retrospective Clinico-Pathological Study. *J Alzheimers Dis*. 2018;63:1317-1323.

14. Ryman SG, Yutsis M, Tian L, et al. Cognition at Each Stage of Lewy Body Disease with Co-occurring Alzheimer's Disease Pathology1. Dugger B, ed. *J Alzheimers Dis*. 2021;80:1243-1256.

15. Budd Haeberlein S, Aisen PS, Barkhof F, et al. Two Randomized Phase 3 Studies of Aducanumab in Early Alzheimer's Disease. *J Prev Alzheimers Dis*. 2022.

16. Liberini P, Valerio A, Memo M, Spano P. Lewy-body dementia and responsiveness to cholinesterase inhibitors: a paradigm for heterogeneity of Alzheimer's disease? *Trends Pharmacol Sci*. 1996;17:155-160.

17. Iturria-Medina Y, Carbonell FM, Evans AC. Multimodal imaging-based therapeutic fingerprints for optimizing personalized interventions: Application to neurodegeneration. *NeuroImage*. 2018;179:40-50.

18. Brown RKJ, Bohnen NI, Wong KK, Minoshima S, Frey KA. Brain PET in Suspected Dementia: Patterns of Altered FDG Metabolism. *RadioGraphics*. 2014;34:684-701.

19. Lim SM, Katsifis A, Villemagne VL, et al. The 18 F-FDG PET Cingulate Island Sign and Comparison to ^{123} I-β-CIT SPECT for Diagnosis of Dementia with Lewy Bodies. *J Nucl Med*. 2009;50:1638-1645.

20. Graff-Radford J, Murray ME, Lowe VJ, et al. Dementia with Lewy bodies: Basis of cingulate island sign. *Neurology*. 2014;83:801-809.

21. Gjerum L, Frederiksen KS, Henriksen OM, et al. Evaluating 2-[18F]FDG-PET in differential diagnosis of dementia using a data-driven decision model. *NeuroImage Clin*. 2020;27:102267.

22. Kantarci K, Boeve BF, Przybelski SA, et al. FDG PET metabolic signatures distinguishing prodromal DLB and prodromal AD. *NeuroImage Clin*. 2021;31:102754.

23. Graff-Radford J, Lesnick TG, Savica R, et al. 18F-fluorodeoxyglucose positron emission tomography in dementia with Lewy bodies. *Brain Commun*. 2020;2:fcaa040.

24. Montine TJ, Phelps CH, Beach TG, et al. National Institute on Aging–Alzheimer's Association guidelines for the neuropathologic assessment of Alzheimer's disease: a practical approach. *Acta Neuropathol (Berl)*. 2012;123:1-11.

25. Hyman BT, Phelps CH, Beach TG, et al. National Institute on Aging–Alzheimer's Association guidelines for the neuropathologic assessment of Alzheimer's disease. *Alzheimers Dement*. 2012;8:1-13.

26. Franklin EE, Perrin RJ, Vincent B, et al. Brain collection, standardized neuropathologic assessment, and comorbidity in Alzheimer's Disease Neuroimaging Initiative 2 participants. *Alzheimers Dement*. 2015;11:815-822.

27. Uchikado H, Lin W-L, DeLucia MW, Dickson DW. Alzheimer Disease With Amygdala Lewy Bodies: A Distinct Form of α-Synucleinopathy. *J Neuropathol Exp Neurol*. 2006;65:685-697.

28. Parkkinen L, O'Sullivan SS, Collins C, et al. Disentangling the Relationship between Lewy Bodies and Nigral Neuronal Loss in Parkinson's Disease. *J Park Dis*. 2011;1:277-286.

29. Balsis S, Benge JF, Lowe DA, Geraci L, Doody RS. How Do Scores on the ADAS-Cog, MMSE, and CDR-SOB Correspond? *Clin Neuropsychol*. 2015;29:1002-1009.

30. Crane PK, Carle A, Gibbons LE, et al. Development and assessment of a composite score for memory in the Alzheimer's Disease Neuroimaging Initiative (ADNI). *Brain Imaging Behav*. 2012;6:502-516.

31. Gibbons LE, Carle AC, Mackin RS, et al. A composite score for executive functioning, validated in Alzheimer's Disease Neuroimaging Initiative (ADNI) participants with baseline mild cognitive impairment. *Brain Imaging Behav*. 2012;6:517-527.

32. Levin F, Ferreira D, Lange C, et al. Data-driven FDG-PET subtypes of Alzheimer's disease-related neurodegeneration. *Alzheimers Res Ther*. 2021;13:49.

33. Apostolova I, Lange C, Suppa P, et al. Impact of plasma glucose level on the pattern of brain FDG uptake and the predictive power of FDG PET in mild cognitive impairment. *Eur J Nucl Med Mol Imaging*. 2018;45:1417-1422.

34. López-González FJ, Silva-Rodríguez J, Paredes-Pacheco J, et al. Intensity normalization methods in brain FDG-PET quantification. *NeuroImage*. 2020;222:117229.

35. Hsieh T-C, Lin W-Y, Ding H-J, et al. Sex- and Age-Related Differences in Brain FDG Metabolism of Healthy Adults: An SPM Analysis. *J Neuroimaging*. 2012;22:21-27.

36. Grothe MJ, Sepulcre J, Gonzalez-Escamilla G, et al. Molecular properties underlying regional vulnerability to Alzheimer's disease pathology. *Brain*. July 2018.

37. Albin RL, Minoshima S, D'Amato CJ, Frey KA, Kuhl DA, Sima AAF. Fluoro-deoxyglucose positron emission tomography in diffuse Lewy body disease. *Neurology*. 1996;47:462-466.

38. Wakabayashi K, Mori F, Takahashi H. Progression patterns of neuronal loss and Lewy body pathology in the substantia nigra in Parkinson's disease. *Parkinsonism Relat Disord*. 2006;12:S92-S98.

39. Brenowitz WD, Hubbard RA, Keene CD, et al. Mixed neuropathologies and associations with domain-specific cognitive decline. *Neurology*. 2017;89:1773-1781.

40. Janvin CC, Larsen JP, Aarsland D, Hugdahl K. Subtypes of mild cognitive impairment in Parkinson's disease: progression to dementia. *Mov Disord Off J Mov Disord Soc*. 2006;21:1343-1349.

41. Torres-Garcia L, P. Domingues JM, Brandi E, et al. Monitoring the interactions between alpha-synuclein and Tau in vitro and in vivo using bimolecular fluorescence complementation. *Sci Rep*. 2022;12:2987.

42. Blazhenets G, Frings L, Sörensen A, Meyer PT. Principal-Component Analysis–Based Measures of PET Data Closely Reflect Neuropathologic Staging Schemes. *J Nucl Med*. 2021;62:855-860.

43. Spires-Jones TL, Attems J, Thal DR. Interactions of pathological proteins in neurodegenerative diseases. *Acta Neuropathol (Berl)*. 2017;134:187-205.

44. Yoo HS, Jeong SH, Oh KT, et al. Interrelation of striatal dopamine, brain metabolism and cognition in dementia with Lewy bodies. *Brain*. March 2022:awac084.

45. Oliveira FPM, Walker Z, Walker RWH, et al. 123I-FP-CIT SPECT in dementia with Lewy bodies, Parkinson's disease and Alzheimer's disease: a new quantitative analysis of autopsy confirmed cases. *J Neurol Neurosurg Psychiatry*. February 2021:jnnp-2020-324606.

46. Shim J-H, Baek H-M. Diffusion Measure Changes of Substantia Nigra Subregions and the Ventral Tegmental Area in Newly Diagnosed Parkinson's Disease. *Exp Neurobiol*. 2021;30:365-373.

47. Bae YJ, Kim J-M, Sohn C-H, et al. Imaging the Substantia Nigra in Parkinson Disease and Other Parkinsonian Syndromes. *Radiology*. 2021;300:260-278.

48. Ballard C, Grace J, McKeith I, Holmes C. Neuroleptic sensitivity in dementia with Lewy bodies and Alzheimer's disease. *Lancet Lond Engl*. 1998;351:1032-1033.

Semiquantitative assessment of the regional loads of Lewy body and tau neuropathology

For a subset of patients (n=45/59; n=41 within our pathological groups; pure-AD=15; AD-LB=20; pure-LB=6) semiquantitative information about the regional loads of Lewy bodies (LBs) and tau neurofibrillary tangles (NFTs) in different brain regions was available. These were reported on a scale from 0 to 4 in the case of LBs (0, none; 1 = <1 LB x10 field; 2 = 1-3 LBs; 3 = 4-10; LB; 4 = >10) and from 0 to 3 for NFTs (0 = no NFTs, 1 = 1-5 NFT/1mm2, 2 = 6-20, 3 = > 20). The available data was used to calculate the average loads of LBs and tau NFTs in limbic and neocortical composite regions. The brain areas sampled for microscopic assessments are reported in Supplementary Table S1, together with their classification into the limbic or neocortical composite and the number of patients with data available for each region (right column). Regions with data for less than 30 patients in our pathological groups were excluded from subsequent analysis (marked in red).

Region	Neuropathology Code	Classification	Patients with data available (n)
Amygdala	L23AMYG	Limbic	41
Entorhinal	L23ENTX	Limbic	41
Hippocampus, CA1	L5CA1	Limbic	41
Hippocampus, Dentate Gyrus	L5DG	Limbic	41
Parahippocampal Gyrus	L5PHG	Limbic	41
Superior and Middle Temporal	L2STG	Neocortical	41
Middle frontal	L1MFG	Neocortical	41
Anterior Cingulate	L19CING	Limbic	41
Precentral Gyrus Motor Cortex	L21MX	-----	25
Inferior Parietal	L3IPL	Neocortical	41
Occipital	L4OL	Neocortical	41
Olfactory Cortex	L6OLFX	----	29
Caudate Putamen	L6PUTC	----	41
Globus Pallidus	L17GP	----	41
Thalamus	L8THAL	----	41
Pontine Base	L11PONS	----	41
Midbrain	L9SN	----	41
Nucleus Basalis Meynert	L17NBM	Limbic	39
Locus Caeruleus	L11LC	----	41
Medulla Oblongata	L12MED	----	40
Cebebellum Dentate Nucleus	L14CBM	----	41
Spinal Cord	L13SC	----	22

Supplementary Table S1: Regions for which semiquantitative information about the regional loads of NFTs and LBs was available. *Marked in red:* Regions with data for less than 30 patients.

Differences in the regional loads of LBs and NFTs between pathological groups

To test whether the differences between groups in the main analyses were related with the severity of pathology, we compared LB and NFT load between neuropathological groups. Results are presented in Suppl. Fig. 1. In statistical analysis, we did not find any significant differences in LB load between the pure-LB and the AD-LB groups (limbic composite: d=-0.35, p=0.394; neocortical composite: d=-0.36, p=0.382; amygdala: d=0.16, p=0.706). Similarly, for tau NFT burden, we did not observe any significant differences between the pure-AD and the AD-LB group (limbic composite: d=0.38, p=0.203; neocortical composite: d=0.20, p=0.505; amygdala: d=0.17, p=0.561).

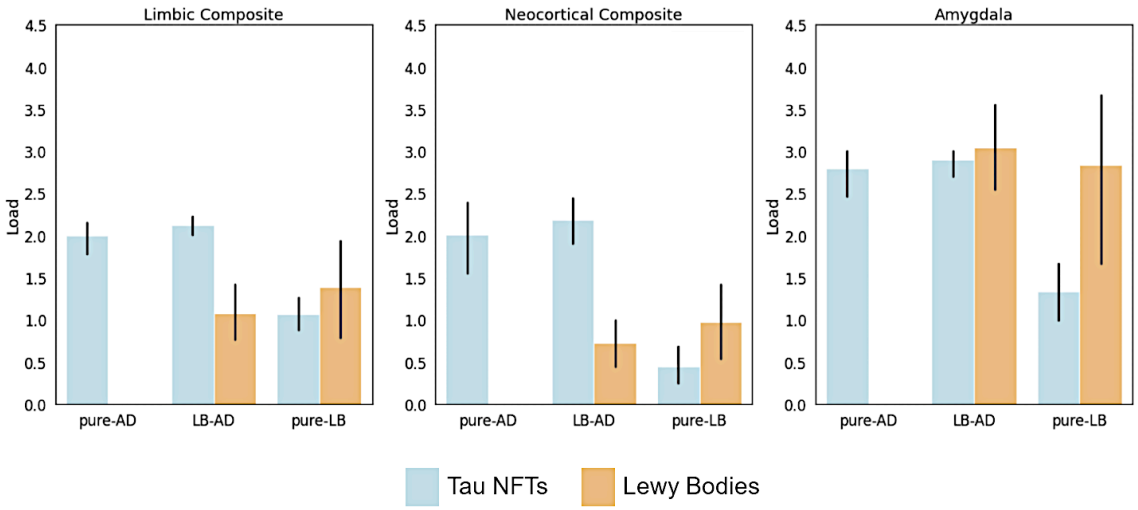

Suppl. Fig. S1: Average regional loads of tau neurofibrillary tangles (NFTs) and Lewy bodies in limbic and neocortical composite regions, as well as in the amygdala separately.

Associations between regional LB loads and cognition

To better understand the role of LBs shaping the differences in cognition between the pathological groups, we evaluated continuous associations of the regional load of LBs in the amygdala and in limbic and neocortical composites with the reported memory performance (ADNI_MEM),

executive performance (ADNI_EXEC) and cognitive profile (Δ (MEM - EXEC)) variables. The correlations were evaluated using Spearman's correlation analysis (with and without controlling for the NFT load) for the whole cohort, and for the AD-LB group alone. Results are shown in Suppl. Table 2. While most of these correlations were not statistically significant, some interesting trends could be observed. Across the whole cohort, the LB load in all regions was negatively correlated with ADNI_MEM, especially when controlling for regional tau NFT load (limbic composite: ρ= -0.34, p=0.03; neocortical composite: ρ= -0.22, p=0.15; amygdala: ρ= -0.22, p=0.16). These associations were not observed for the AD-LB group alone, where the only remarkable finding was a correlation between Δ (MEM-EXEC) and amygdala LBs at trend-level statistical significance (ρ= 0.40, p=0.09), suggesting that these might help to shape a more executive phenotype within the AD-LB group.

		Cognitive Score					
		ADNI_MEM		**ADNI_EF**		**Δ (MEM-EXEC)**	
		ρ (p)	**Partial ρ*, (p)**	**ρ (p)**	**Partial ρ*, (p)**	**ρ (p)**	**Partial ρ*, (p)**
		Results for the whole cohort					
Region Lewy Body Load	**Limbic**	-0.19 (0.20)	-0.34 (0.03)	-0.09 (0.56)	-0.15 (0.35)	-0.10 (0.54)	-0.15 (0.37)
	Neocortical	-0.09 (0.56)	-0.22 (0.15)	-0.13 (0.43)	-0.18 (0.26)	0.01 (0.97)	-0.02 (0.90)
	Amygdala	-0.21 (0.18)	-0.22 (0.16)	-0.10 (0.53)	-0.11 (0.52)	-0.10 (0.53)	-0.12 (0.47)
		Results for the AD-LB group					
Region Lewy Body Load	**Limbic**	0.15 (0.51)	0.08 (0.72)	0.22 (0.36)	0.15 (0.54)	-0.10 (0.70)	-0.06 (0.80)
	Neocortical	0.10 (0.67)	0.18 (0.45)	-0.01 (0.96)	0.04 (0.86)	0.05(0.85)	-0.05 (0.84)
	Amygdala	0.23 (0.33)	0.25 (0.28)	-0.02 (0.93)	-0.13 (0.59)	0.24 (0.30)	0.40 (0.09)

Suppl. Table S2: Associations between cognitive scores (ADNI_MEM, ADNI_EF, Δ (MEM-EXEC)) and neuropathologically assessed regional loads of LBs across different regions of interest

in the whole cohort and separately in the AD-LB group. * indicates partial Spearman correlation using the regional tau NTF load as a covariate

Associations of the regional loads of NFTs and LBs with FDG-PET

Following up on the observed associations of Braak stage and SNnl with the CISr, occipital SUVR and MTL SUVR (see Fig. 4 of the main manuscript), we tested whether similar associations were also found when using regional loads of tau NTFs and LBs as neuropathologic markers. Similar to Braak tau stages, both limbic and neocortical NFTs were significantly associated with a lower CISr (ρ=-0.341, p=0.027; ρ=-0.31, p=0.047) and lower MTL SUVR (ρ=-0.40 p=0.009; ρ=-0.44 p=0.003), but not with occipital metabolism (ρ=0.14, p=0.364; ρ=0.07, p=0.639; Supplementary Figure S2). However, in contrast to SNnl, limbic, neocortical and amygdala regional LB loads were not significantly associated with the CISr (ρ=0.04, p=0.782; ρ=0.11 p=0.510; ρ=0.02, p=0.905) or MTL (ρ=0.14, p=0.398, ρ=0.19, p=0.241; ρ=0.09, 0.564), although trend-level negative correlations were found between regional LB load and lower occipital SUVR (ρ=-0.30, p=0.060, ρ=-0.27, p=0.084; ρ=-0.26, p=0.108) (Supplementary Figure S3).

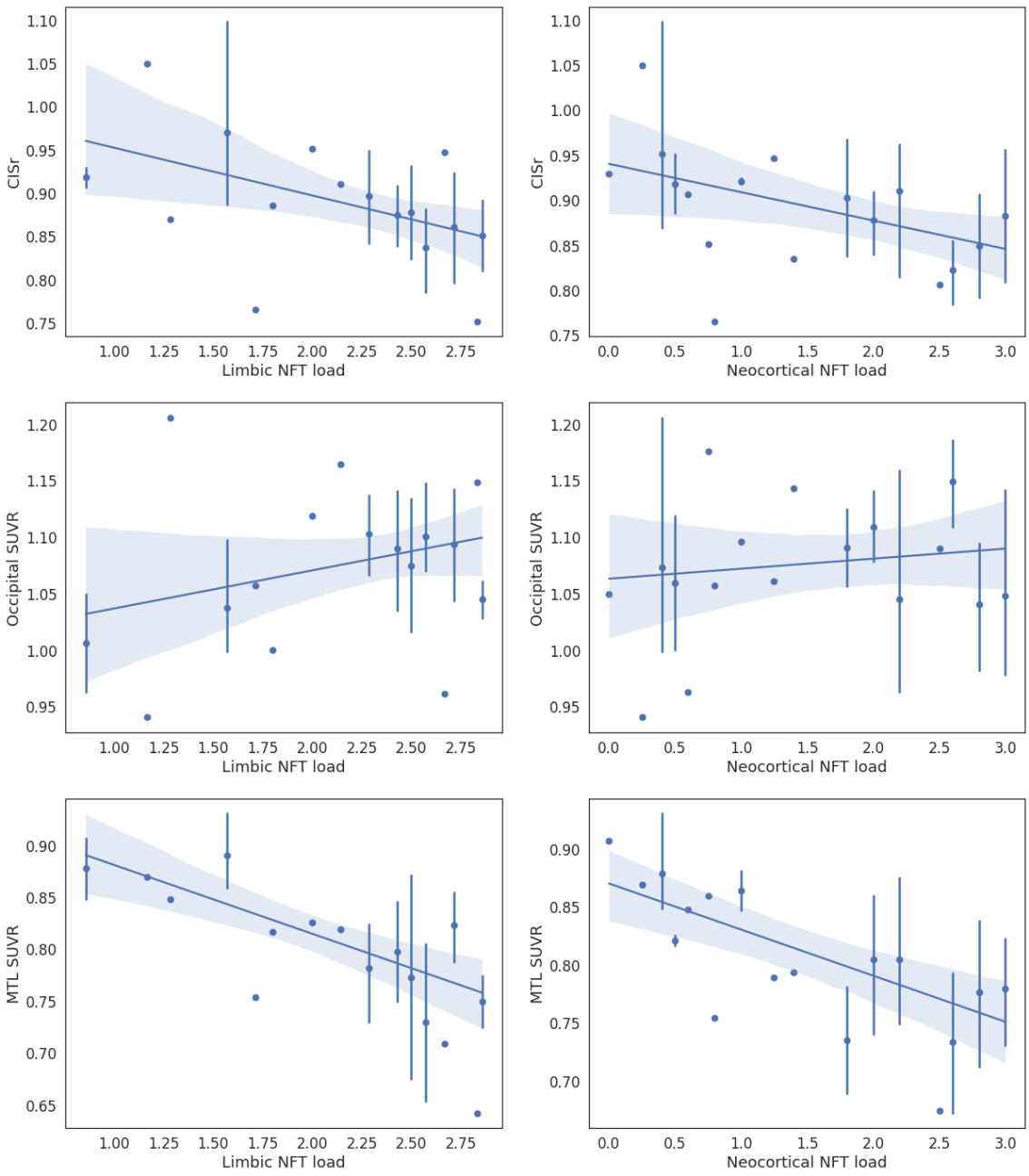

Suppl. Fig. S2: Associations between limbic (left) and neocortical (right) tau NFT loads and different FDG-PET ROI features: CISr (top), occipital SUVR (center) and MTL SUVR (bottom).

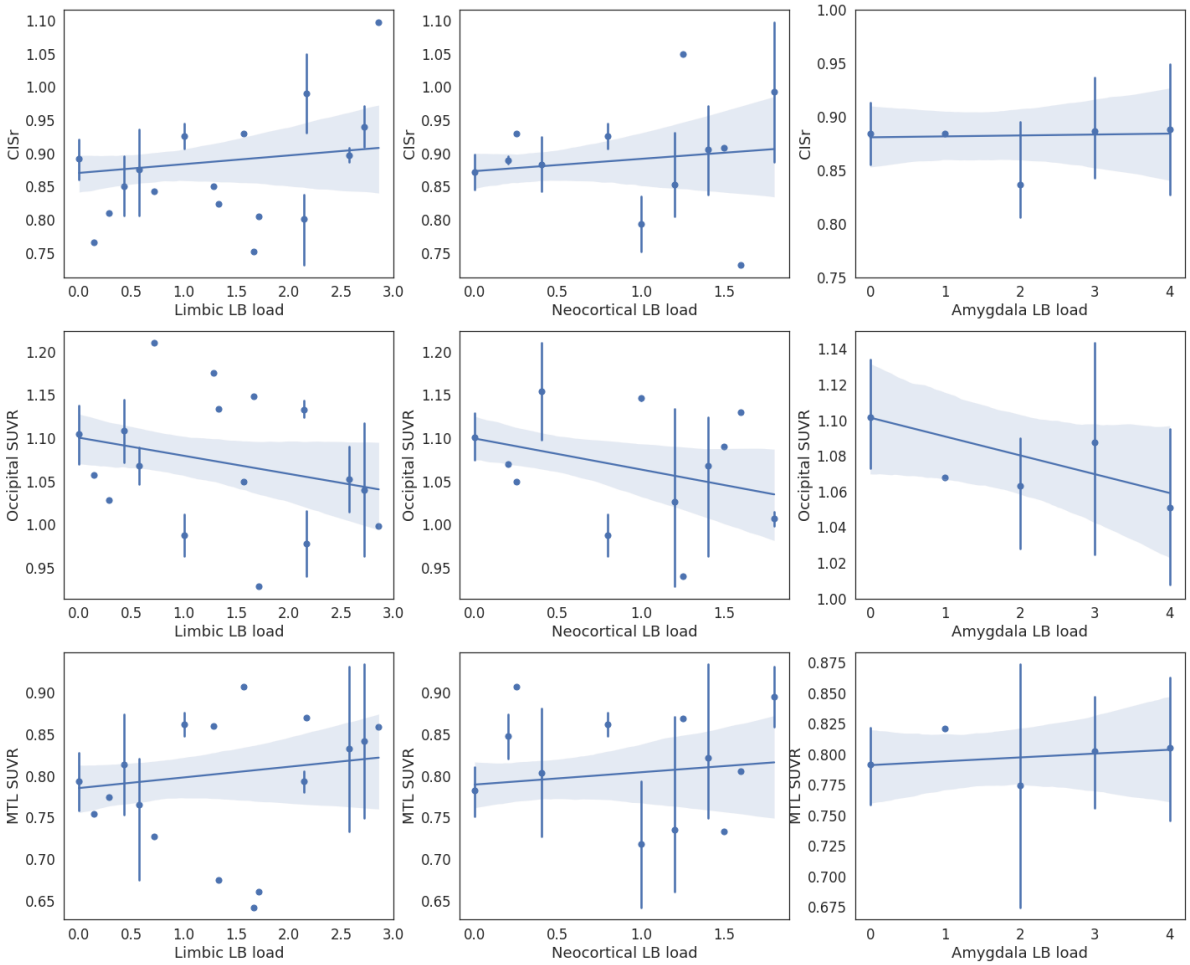

Suppl. Fig. S3: Associations between limbic (left), neocortical (center) and amygdala LB loads and different FDG-PET ROI features: CISr (top), occipital SUVR (center) and MTL SUVR (bottom).